The effect of long-range strain fields on transport properties of disclinated materials

2001 J. Phys.: Condens. Matter 13 1023

(http://iopscience.iop.org/0953-8984/13/5/316)

INSTITUTE OF PHYSICS PUBLISHING JOURNAL OF PHYSICS: CONDENSED MATTER

J. Phys.: Condens. Matter **13** (2001) 1023–1040 www.iop.org/Journals/cm PII: S0953-8984(01)15004-6

The effect of long-range strain fields on transport properties of disclinated materials

S E Krasavin and V A Osipov

Joint Institute for Nuclear Research, Bogoliubov Laboratory of Theoretical Physics, 141980 Dubna, Moscow Region, Russia

E-mail: osipov@thsun1.jinr.ru and krasavin@thsun1.jinr.ru

Received 26 June 2000

Abstract

The problem of both phonon and electron scattering by long-range strain fields caused by wedge disclination dipoles (WDD) is studied in the framework of the deformation potential approach. The exact analytical results for the mean free path are obtained within the Born approximation. The WDD-induced contribution to the residual resistivity in nanocrystalline metals is estimated. Phonon scattering due to randomly distributed WDDs is shown to result in a clear crossover from T^3- to T^2-behaviour in the thermal conductivity, κ, at low temperatures. A combination of two scattering processes, the phonon scattering due to biaxial WDD and the Rayleigh-type scattering, is suggested to be of importance for amorphous dielectrics. Our results are in good agreement with the experimentally observed κ for a-SiO_2, a-GeO_2, a-Se, and polystyrene. Numerical calculations show that κ is very sensitive to the size of the dipole separation, which is fixed near 20 Å.

1. Introduction

There exist many varieties of extended defect in crystals, topological in their origin. The best-known examples are dislocations, disclinations, twins, grain boundaries, and stacking faults. These defects play a significant role in the description of various phenomena in real crystals as well as in disordered materials. In particular, there is reason to believe that linear defects like dislocations and disclinations are the principal imperfections of liquid crystals (Kléman 1983), some amorphous solids (Nelson 1983, Rivier 1979), and polymers (Li and Gilman 1970).

The contribution to the transport characteristics due to dislocations is now well understood (see for example Ziman (1960), Gantmakher and Levinson (1987)). Some aspects of the qualitative behaviour of the disclination-induced electron scattering have been recently presented by Krasavin and Osipov (1997). In particular, it was found that both dislocations and disclinations can be effective scattering centres for conduction electrons, especially at low temperatures when other scattering mechanisms are suppressed. Thus, along with point impurities, these defects give a contribution to the residual resistivity. In real crystals, however,

0953-8984/01/051023+18$30.00

the isolated disclinations are rather exotic objects. Instead, for topological reasons, the dipole as well as multipole configurations are more favourable. In addition, the creation energy for a single disclination considerably exceeds that for a disclination dipole.

There is another reason to call attention to dipoles of disclinations. In fact, the wedge disclination dipoles (WDD) *simulate* finite dislocation walls. In turn, the low-angle grain boundaries can be described as dislocation walls (Read and Shockley 1950, Amelinckx 1959). Thus, one can expect the results obtained for disclination dipoles to be useful in description of the grain-boundary scattering problem. This allows us to extend the possible applications to a study of the transport properties in materials where grain boundaries are of importance (e.g., in polycrystals). In particular, there is experimental evidence that the grain boundaries give a contribution to the resistivity in metals (see for example Gusev (1998)), which depends on the size of the grain boundary. Notice that although the problem of the grain-boundary-induced scattering was formulated many years ago, a proper solution is still lacking.

A theory of the phonon scattering by grain boundaries has been developed within the Born approximation (Klemens 1955). A grain boundary was considered as a wall of edge dislocations with the rather strong assumption that the dislocation wall is *infinitely* long. Nevertheless, the main properties predicted by this model have been confirmed by experiments (Berman 1952, Anderson and Malinowski 1972, Roth and Anderson 1978). In particular, the phonon mean free path was found to be constant over a wide temperature range. As a result, the low-temperature thermal conductivity in materials with grain boundaries varies as T^3 in agreement with the experimental data.

Recently (Osipov and Krasavin 1998a), the grain-boundary phonon scattering problem was investigated within a more realistic model which takes into account the finiteness of the boundary. The basis for this model was the above-mentioned analogy between disclination dipoles and *finite* walls of edge dislocations (Li 1972, de Wit 1973). It was found that the proper consideration of the finiteness of the boundary results in a low-temperature crossover (from T^3 to T^2) of the thermal conductivity. The crossover temperature depends crucially on the dipole separation. Notice that a similar crossover has been found in a number of experiments on deformed alkali halides (Anderson and Malinowski 1972, Roth and Anderson 1978) and ferroelectric KDP (Weilert *et al* 1993) (see the discussion below).

A more intriguing application is an attempt to describe the physics of dielectric glasses by considering WDD as the principal defects in these materials (Osipov and Krasavin 1998b). In other words, this is an attempt to go beyond effective-medium models and take into account the microscopic structure of glasses. In fact, the disclinations and dipoles of disclinations have already been considered in the context of disordered systems (Kléman 1989, Nelson 1983). What is important is that these defects are known to be sources of additional long-range strain fields. Moreover, it was found recently that the phonon scattering due to strain fields caused by biaxial WDD (BWDD) becomes very specific and, at small dipole separation $2L$, one can fit the thermal conductivity in a-SiO_2 below 1 K in good agreement with experiment. This consideration introduces the new dimensional parameter, $2L$, which characterizes the microstructure of glasses with BWDDs as the basic elements of disordered states.

It is also interesting to note that this approach supports the cluster picture of glasses (Kauzmann 1948, Phillips 1983). Indeed, according to this picture, in the amorphous state there exist many microclusters with average diameters of the order of 20–30 Å. The strain fields due to cluster interfaces in a network can be rigorously defined in terms of finite dislocation walls or, equivalently, BWDDs. Notice that for a-SiO_2 the best fit was obtained with $2L = 20$ Å which is in a good agreement with the cluster diameter proposed within the cluster model as well as with the results of other experiments.

On the other hand, the concept of elastic dipoles for orientational glasses was introduced and successfully explored by Randeria and Sethna (1988) and Grannan *et al* (1988, 1990a, b). The authors considered elastic dipoles as structural elements of glasses additional to two-level systems (TLS). This assumption allows them to describe both the specific heat and the thermal conductivity of some glasses in the plateau region and above (up to 100 K). The physical nature of these dipoles, however, has not yet been clarified. It will be shown below that the concept of the elastic dipole can be successfully realized via dipoles of wedge disclinations without considering TLS. That is, the WDD-induced phonon scattering is found to provide the correct description of the low-temperature thermal conductivity of various amorphous dielectrics.

The main goal of the paper is twofold. First, we outline the general formalism of the WDD-induced scattering for both electrons and phonons. The most important details needed for a better understanding of the calculations are given. Second, we apply the results obtained in the description of two important problems. The first one is the experimentally observed deviation of the thermal conductivity from a T^3-dependence below some T' for deformed materials. The second problem is the thermal conductivity of amorphous dielectrics.

It was shown (Osipov and Krasavin 1998b) that the experimentally observed behaviour of the thermal conductivity of a-SiO_2 over a wide temperature range can be explained by a combination of two scattering processes. The first one arises from the phonon scattering due to biaxial WDD while the second one is the Rayleigh-type scattering. In the present paper we extend our investigation to other glasses and discuss some unresolved questions.

The paper is organized as follows. The general formalism of the WDD-induced scattering is presented in section 2. We consider all possible types of WDD and calculate the corresponding phonon mean free paths. The principal distinction between the scattering properties of the uniaxial and biaxial dipoles is shown. In subsection 2.1 the approach developed is applied to estimation of the WDD-induced contribution to the residual resistivity of granular metals. In subsection 2.2 the phonon scattering due to WDD is studied and the contribution to the thermal conductivity is calculated. In section 3 we apply the WDD-induced mechanism of phonon scattering to the problem of thermal conductivity in amorphous dielectrics. The results are compared with the experimentally observed κ for a-SiO_2, a-GeO_2, a-Se, and polystyrene (PS). Section 4 is devoted to the detailed discussion of the results obtained, specifically with relation to the proposed WDD-based model for dielectric glasses.

2. Theory of the WDD-induced scattering

In this section we study the contribution to the effective cross-section which comes from the potential associated with a static deformation of a lattice caused by straight WDD. Two reasonable approximations are in common usage in studies of such problems (see for example Ziman (1960), Gantmakher and Levinson (1987)). First, we suppose that the scattering processes are elastic and, second, that the Born approximation is valid. Also, we will consider here the simplest case where the only elastic deformations are dilatations.

In this case, the effective perturbation energy due to the strain field caused by a single WDD takes the form

$$U(\boldsymbol{r}) = G \operatorname{Tr} E_{ij} \tag{1}$$

where $\operatorname{Tr} E_{ij}$ is the trace of the strain tensor due to WDD and G is an interaction constant.

Let the disclination lines be oriented along the z-axis and the position of the positive disclination be $(0, -L)$ (see figure 1). Notice that in the general case the axes of rotations (with $\boldsymbol{\Omega}_1 = \Omega \boldsymbol{e}_z$ and $\boldsymbol{\Omega}_2 = -\Omega \boldsymbol{e}_z$) are shifted relative to their positions by arbitrary distances l_1 and l_2, respectively. For $l_1 = l_2 = 0$ one gets the biaxial WDD with non-skew axes of

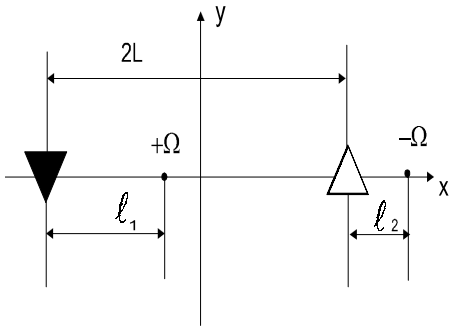

Figure 1. A schematic picture of a wedge disclination dipole with axes of rotation shifted by distances l_1 and l_2. The disclination lines are oriented along the z-axis for both defects

rotation. It was shown (Li 1960) that this dipole can be simulated by a finite wall of edge dislocations with parallel Burgers vectors. In particular, the far strain fields caused by biaxial WDD agree with those from a finite dislocation wall (de Wit 1973).

For $l_1 - l_2 = 2L$ and $l_1 = -l_2$ one gets the uniaxial and the symmetrical uniaxial WDD, respectively. Notice that uniaxial WDD can be simulated by a finite wall of edge dislocations complemented by two additional edge dislocations at both ends of the wall. The sign of these dislocations is opposite to that of the dislocations in the wall, and the absolute values of the Burgers vectors are equal to $b = 2L\tan(\Omega/2)$ ($b = b_y$ for the chosen geometry). As a result, the uniaxial WDD becomes a strongly screened system as opposed to the biaxial WDD (see figure 2). In the general case, $l_1 \neq l_2 \neq 0$, one gets the biaxial WDD with shifted axes of rotation.

Substituting the explicit form of E_{ij} into equation (1) (see appendix A) we find for the perturbation energy $U(\boldsymbol{r})$

$$U(x, y) = B\left[\frac{1}{2}\ln\frac{(x+L)^2+y^2}{(x-L)^2+y^2} - l_1\frac{x+L}{(x+L)^2+y^2} + l_2\frac{x-L}{(x-L)^2+y^2}\right] \quad (2)$$

where $B = G\nu(1-2\sigma)/(1-\sigma)$, $\nu = \Omega/2\pi$ is the Frank index, and σ is the Poisson constant. Notice that all possible types of WDD are included in equation (2).

As is seen from equations (A.1) and (A.2) given in the appendix, all strains caused by WDD are located in the xy-plane. In this case, the only components of the wavevector that are normal to the defect lines, $\boldsymbol{q} = \boldsymbol{q}_\perp$, are involved in the scattering process. For the sake of simplicity, let us assume that carriers are incident normally to disclination lines.

The problem reduces to the two-dimensional case with the mean free path given by

$$\Lambda^{-1} = n_i\int_0^{2\pi}(1-\cos\theta)\mathcal{R}(\theta)\,\mathrm{d}\theta. \quad (3)$$

Here $\mathcal{R}(\theta)$ is an effective differential scattering radius, and n_i is the areal density of WDD. Notice that when the axes of WDD are oriented randomly, one has to perform an additional averaging over all possible angles of incidence. As was shown for dislocations (Gantmakher and Levinson 1987), however, such averaging leads merely to a modification of the numerical factor in $\mathcal{R}(\theta)$.

Within the Born approximation, $\mathcal{R}(\theta)$ is determined to be (Ziman 1960)

$$\mathcal{R}(\theta) = \frac{qS^2}{2\pi\hbar^2 v^2}\overline{|\langle\boldsymbol{q}|U(\boldsymbol{r})|\boldsymbol{q}'\rangle|^2} \quad (4)$$

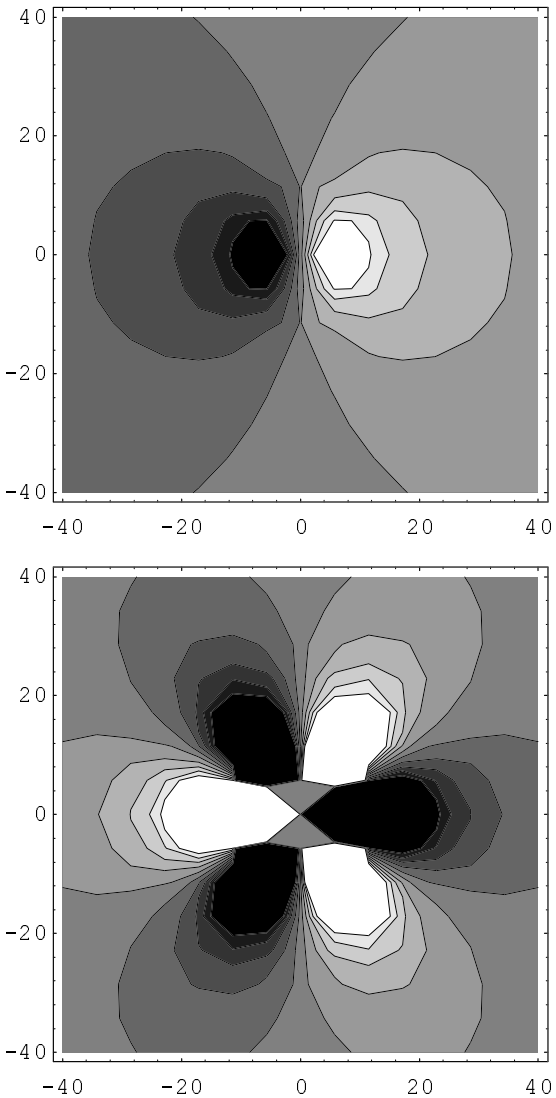

Figure 2. A contour plot of the perturbation energy (2), $U(x, y)/B$ (in Å), for biaxial WDD ($l_1 = l_2 = 0$, upper picture) and for uniaxial WDD ($l_1 - l_2 = 2L$, lower picture).

where all vectors are two dimensional, S is a projected area, v is the magnitude of the carrier velocity. The bar denotes averaging over α which is the angle between $\boldsymbol{p} = \boldsymbol{q} - \boldsymbol{q}'$ and the x-axis; in other words, it means the averaging over randomly oriented dipoles in the xy-plane. Evidently, the problem reduces to the estimation of the matrix element in equation (4) with the potential from equation (2). For this purpose, it is convenient to use the polar coordinates (r, φ):

$$U(p, \alpha) = \langle \boldsymbol{q}|U(\boldsymbol{r})|\boldsymbol{q}'\rangle = \frac{1}{S}\int \mathrm{d}^2 r \ \exp[\mathrm{i}pr\cos(\varphi - \alpha)]U(r, \varphi). \tag{5}$$

For elastic scattering, the matrix element in equation (5) depends only on $|\boldsymbol{q}| = |\boldsymbol{q}'|$ and the scattering angle θ. Thus, $p = |\boldsymbol{p}| = |\boldsymbol{q} - \boldsymbol{q}'| = 2q\sin(\theta/2)$.

After the integration in equation (5) and following averaging of $|U(p,\alpha)|^2$ with respect to α, one obtains (see the details in appendix B)

$$\mathcal{R}(\theta) = \frac{\pi B^2}{\hbar^2 v^2 \sin(\theta/2)} \left\{ \frac{2}{p^3}\big(1 - J_0(2pL)\big) + \frac{\Delta_l^2}{2p}\left(\frac{1}{2} + J_0(2pL) - \frac{J_1(2pL)}{2pL}\right) - \frac{2\Delta_l}{p^2} J_1(2pL) \right\} \tag{6}$$

where $\Delta_l = l_1 - l_2$ and $J_n(t)$ are the Bessel functions. Upon integrating equation (3) with respect to θ one finally obtains

$$\Lambda^{-1} = \frac{B^2 L^2 \pi^2 n_i}{q\hbar^2 v^2} \left\{ z^2 \left(\frac{1}{2} + J_0^2(2qL)\right) + \left(8 - \frac{z(z+8)}{2}\right)(J_0^2(2qL) + J_1^2(2qL)) - \frac{4}{qL} J_0(2qL) J_1(2qL) \right\} \tag{7}$$

where $z = \Delta_l / L$. It should be emphasized that equation (7) is the exact result which allows us to describe all types of WDD. Notice that the behaviour of Λ in equation (7) is actually governed by the parameter $2L$.

Let us consider two important limiting cases. For biaxial dipoles with $\Delta_l = 0$ ($z = 0$) one obtains

$$\Lambda_{bi}^{-1} = \frac{8B^2 L^2 n_i \pi^2}{q\hbar^2 v^2} \left\{ J_0^2(2qL) + J_1^2(2qL) - \frac{1}{2qL} J_0(2qL) J_1(2qL) \right\}. \tag{8}$$

For uniaxial dipoles $\Delta_l = 2L$ ($z = 2$), and the mean free path Λ is

$$\Lambda_{uni}^{-1} = \frac{2B^2 L^2 n_i \pi^2}{q\hbar^2 v^2} \left\{ 1 + J_0^2(2qL) - J_1^2(2qL) - \frac{2}{qL} J_0(2qL) J_1(2qL) \right\}. \tag{9}$$

In what follows, we apply the formalism developed to the problem of the WDD-induced electron and phonon scattering.

2.1. Electron scattering: WDD-induced residual resistivity in metals

As is known (Ziman 1960), the residual resistivity of metals may be caused by electron scattering due to linear defects like dislocations, stacking faults, and grain boundaries. It was mentioned in the introduction that the WDD-based model is a good candidate for modelling the grain boundaries. Thus, the previous analysis allows us to study the contribution to the residual resistivity due to grain boundaries.

Let us use the well-known Drude formula for the resistivity in the static regime:

$$\rho = \left(\frac{m}{ne^2}\right)\left\langle \frac{1}{\tau} \right\rangle \tag{10}$$

where τ is the relaxation time, m and e are the mass and the charge of the conduction electron, and n is the electron density. For point impurities and linear defects like dislocations and disclinations, the angle brackets denote the configurational average. In our case, this is the averaging over α in equation (4). Thus, one can write the final result

$$\rho = \left(\frac{m v_F}{ne^2}\right)\Lambda^{-1} \tag{11}$$

with Λ from equation (7), where $q = q_F$, $v = v_F$, and $G = G_d$. Obviously, the index F denotes the Fermi values, and $G_d \simeq (2/3)E_F$ is the deformation potential constant (Ziman 1960), where E_F is the Fermi energy. For simplicity, we restrict our consideration to metals

with a parabolic zone where the minimum lies in the centre of the Brillouin band. For metals, typically $q_F \approx 0.6$–1.2 Å^{-1}. The dipole separation is chosen to be $2L \approx 10^2$–10^4 Å, which is of the order of the grain size in polycrystals. In this case, $2q_F L \gg 1$ and, consequently, the Bessel functions in equation (7) can be approximated by their asymptotic values. The results are as follows:

$$\rho_{bi} = 16B_e^2 \pi L n_i / n e^2 m v_F^3 \tag{12}$$

and

$$\rho_{uni} = 2B_e^2 \pi^2 L^2 n_i / n e^2 \hbar v_F^2 \tag{13}$$

where $B_e = B(G = G_d)$.

The main difference between the behaviours of ρ_{bi} and ρ_{uni} comes from their L-dependences. As is seen, at fixed n_i, $\rho_{bi} \sim L$ while $\rho_{uni} \sim L^2$. As a result, ρ_{bi} is found to be larger than ρ_{uni}. This agrees with the above-mentioned properties of these dipoles. In the case of biaxial WDD, the main contribution is seen to come from the low-angle scattering processes, in view of the long-range character of the perturbation energy in equation (2). In contrast, for uniaxial WDD the large-angle scattering dominates, since they are strongly screened systems (see figure 2). In particular, at $2L \sim 10^3$–10^4 Å, $n_i \sim 10^9$ cm^{-2}, and $\nu = 0.01$, one obtains $\rho_{bi} \sim 10^{-12}$–10^{-11} Ω cm while $\rho_{uni} \sim 10^{-9}$–10^{-7} Ω cm. Notice that the value of ρ_{uni} agrees with that in the case of edge dislocations of a similar density (Rider and Foxon 1967, Blewitt *et al* 1954).

It should be noted that the experiments show an increase of the residual resistivity of nanocrystalline metals with L decreasing (Gusev 1998). This can be explained within the above-proposed model as due to the direct L-dependence of n_i. Indeed, it is reasonable to assume that $n_i \sim L^{-p}$ with $1 < p \leqslant 2$ (usually $p = 2$). Thus, in accordance with equation (12), ρ_{bi} increases with decreasing L. It is interesting to note that in this case ρ_{uni} decreases with L (except for $p = 2$), as is seen from equation (13). Let us reiterate that only the biaxial WDD with non-skew axes of rotations (BWDD) simulate the grain boundary.

2.2. Phonon scattering: low-temperature heat transport

It is clear that phonon scattering due to WDD also affects the low-temperature thermal conductivity, κ. We start from the well-known kinetic formula

$$\kappa = \frac{1}{3} \int_0^{\omega_D} C(\omega, T) v_s l(\omega, T)\, \mathrm{d}\omega \tag{14}$$

where $C(\omega, T)\, \mathrm{d}\omega$ is the specific heat contributed by acoustic phonons within the frequency interval $\mathrm{d}\omega$, v_s is an average phonon velocity, and $l(\omega, T)$ is the phonon mean free path. It is suggested that $C(\omega, T)$ has the standard form with a density of states quadratic in ω and the Debye cut-off ω_D.

The effective perturbation energy caused by the strain field of WDD is determined as $U(\boldsymbol{r}) = \hbar\omega\gamma \operatorname{Tr} E_{AB}$ (Ziman 1960, Klemens 1955), where $\hbar\omega$ is the phonon energy with wavevector $\boldsymbol{q}$, $\omega = q v_s$, v_s is the velocity of sound (for simplicity it is assumed that the three acoustic branches are equivalent), and γ is the Grüneisen constant. As previously, we suppose that the phonons are incident normally to the disclination lines, so that we deal with a two-dimensional scattering problem. The principal difference from the case of electron scattering is the explicit q-dependence of the perturbation energy (see for example Ziman (1960)). That is, the strain tensor due to the WDD remains the same while the coefficient B in equation (2) should be replaced by $B_{ph} = \hbar q v_s \gamma \nu (1 - 2\sigma)/(1 - \sigma)$. Equations (4) and (5) preserve their form in this case as well.

For BWDD the phonon mean free path is found to be (Osipov and Krasavin 1998b)

$$l_{bi}^{-1} = 2D^2(2\nu L)^2 n_i q\left(J_0^2(2qL) + J_1^2(2qL) - \frac{1}{2qL}J_0(2qL)J_1(2qL)\right) \tag{15}$$

where $D = \pi\gamma(1-2\sigma)/(1-\sigma)$. For uniaxial WDD one obtains

$$l_{uni}^{-1} = \frac{D^2}{2}(2\nu L)^2 n_i q\left(1 + J_0^2(2qL) - J_1^2(2qL) - \frac{2}{qL}J_0(2qL)J_1(2qL)\right). \tag{16}$$

Figure 3 shows $l(\omega)$ for three types of WDD. We have used a size of the grain boundary of $2L = 2700$ Å, which is typical for polycrystals. As is seen, the three curves behave differently. At low frequencies the scattering by uniaxial WDD resembles that by a point impurity. That is, it strongly depends on ω: $l_{uni} \sim \omega^{-5}$, thus once again confirming the view of uniaxial WDD as a strongly screened system. At high frequencies, uniaxial dipoles scatter phonons like dislocations with $l_{uni} \sim \omega^{-1}$. It is interesting that the same ω^{-1}-dependence appears for arbitrary biaxial dipoles both at low and high frequencies. What is more important, there is only one type of biaxial dipole, BWDDs, which show unique behaviour with $l_{bi} \to$ constant as ω increases (see figure 3). It was found (Osipov and Krasavin 1998a) that the change in behaviour of l_{bi} occurs at $2qL \sim 1$ or, equivalently, at $\omega^* \sim v_s/2L$. Thus, in the dominant-phonon approximation the crossover temperature T' is defined by

$$T' \approx \hbar v_s/2Lk_B. \tag{17}$$

It should be emphasized that this intriguing result provides the basis for the following important speculations. Notice that some visible irregularities in figure 3 arose from rapid oscillations of the Bessel functions near the characteristic frequency ω^*.

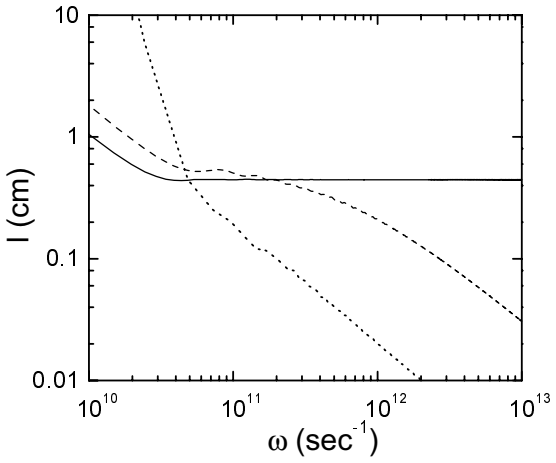

Figure 3. The phonon mean free path $l(\omega)$ at $2q_DL = 6 \times 10^3$ for $\Delta_l = 0$ (solid line), $\Delta_l = 2L$ (dotted line), and $\Delta_l = 0.5L$ (dashed line). The parameter set used is: $L = 1.35 \times 10^{-5}$ cm, $\nu = 0.023$, $D = 2.6$, $n_i = 1.8 \times 10^7$ cm^{-2}, and $v_s = 4.8 \times 10^5$ cm s^{-1}.

A contribution to the thermal conductivity caused by the phonon scattering due to static WDD can be obtained by integration of equation (14) using the phonon mean free path from equations (15) and (16). As was shown by Osipov and Krasavin (1998a), only the thermal conductivity with l_{bi} from equation (15) exhibits a crossover from $\kappa \sim T^2$ to $\kappa \sim T^3$ at low temperatures. It should be emphasized that such behaviour of $\kappa(T)$ is specific to BWDD (which simulate a finite wall of edge dislocations). For example, for the uniaxial dipoles one

obtains that $\kappa \sim T^{-2}$ at low temperatures and $\kappa \sim T^{-1}$ for $T \to \Theta_D$, where Θ_D is the Debye temperature. The result of the calculations is shown in figure 4 for the chosen model parameters. Notice that $\kappa(T)$ depends essentially on $2L$ in accordance with equation (17). In particular, the solid curve in figure 4 (for $2L = 2000$ Å) corresponds to $T' \sim 0.1$ K.

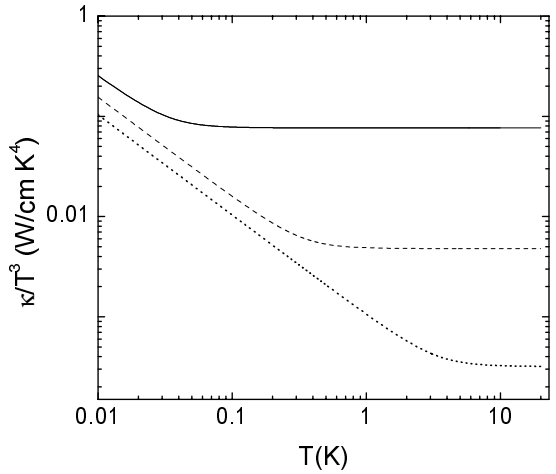

Figure 4. Reduced thermal conductivity due to biaxial WDD scattering, κ/T^3, versus temperature T, calculated according to equation (14). The parameter set used is: $L = 1 \times 10^{-5}$ cm, $n_i = 1.25 \times 10^7$ cm^{-2} (solid line); $L = 1 \times 10^{-6}$ cm, $n_i = 2 \times 10^9$ cm^{-2} (dashed line); $L = 1 \times 10^{-7}$ cm, $n_i = 3 \times 10^{11}$ cm^{-2} (dotted line). The rest of the parameter set: $\nu = 0.023$, $v_s = 4.8 \times 10^5$ cm s^{-1}, $\Theta_D = 350$ K, $D = 2.6$, is the same for each curve.

It should be mentioned that a similar low-temperature crossover has been observed in both undeformed and plastically deformed alkali halides (Anderson and Malinowski 1972, Roth and Anderson 1978) as well as in ferroelectric KDP crystals (Weilert *et al* 1993). For undeformed single LiF crystals the crossover has been explained by phonon scattering on the sample surfaces. Two important questions, however, were left open: (i) why the thermal conductivity behaves like T^2 below T'; and (ii) why the crossover temperature lies near 0.1–0.2 K. Moreover, in ferroelectric KDP crystals with fixed number of domain walls, the same crossover is well pronounced in both cases: when surface scattering was taken into account and when it was subtracted, so only the grain-boundary scattering was effective. Surprisingly, the crossover temperatures in these experiments were found to be exactly the same: $T' \sim 0.2$ K. To our knowledge, there is still no satisfactory explanation of these phenomena.

In accordance with our results, the very appearance of a crossover from T^3 to T^2 at low temperatures should indicate that a crystal contains either grain boundaries or rotational defects like disclinations and/or disclination dipoles of a certain kind (which means a disordered state).

3. BWDD in dielectric glasses: thermal conductivity

There are two important consequences of the previous section. First, it was found that the BWDD-induced contribution to the thermal conductivity behaves like T^2 at very low temperatures. As is well known (Zeller and Pohl 1971), this behaviour is peculiar to dielectric glasses, where $\kappa \sim T^2$ for $T < 1$ K. Second, the critical temperature T' depends considerably on the size of the dipole separation (the length of the wall of the edge dislocations). In particular, one obtains $T' \sim 1$ K at $2L \sim 20$ Å (see also figure 4). It is intriguing that exactly the same

values are expected within the cluster model proposed for dielectric glasses (Phillips 1981a, b).

This finding has stimulated a detailed study of the problem. It was shown by Osipov and Krasavin (1998b) that the experimental data for the thermal conductivity in vitreous silica (a-SiO_2) can be explained by a combination of two scattering processes. The first one comes from the sound wave scattering due to BWDD while the second one is known as Rayleigh-type scattering, which appears due to the local variations in structure. In this section, we present the model and extend the analysis to other glasses.

In accordance with our scenario, the mean free path is determined to be

$$l(\omega) = (l_{bi}^{-1} + l_{struc}^{-1})^{-1} \tag{18}$$

where l_{bi} comes from equation (15), and l_{struc} should be taken in the most general form, describing the Rayleigh scattering over the complete frequency range. The interpolation formula reads (see for example Jones *et al* (1978))

$$l_{struc} = Y^{-1}\left(\frac{\hbar\omega}{k_B}\right)^{-4} + l_0 \tag{19}$$

where Y is a constant which has been considered as a fitting parameter, and l_0 is the high-frequency limit. Figure 5 shows l_{bi}, l_{struc}, and $l(\omega, T)$ with the model parameters for a-SiO_2 taken from table 1. One can see that $l(\omega)$ has a form typical for glassy materials. At low frequencies, $\omega < 10^{12}$ s^{-1}, $l(\omega) \sim \omega^{-1}$, and the main contribution is due to the BWDD-induced scattering. In the intermediate region, both scattering processes are involved, while at high frequencies, the Rayleigh scattering becomes dominant. Notice that the region 10^{12} s^{-1} $< \omega < 10^{13}$ s^{-1} is responsible for the plateau in the thermal conductivity. We have found (Osipov and Krasavin 1998b) that the size of this region decreases with increase of $2L$ and/or l_0.

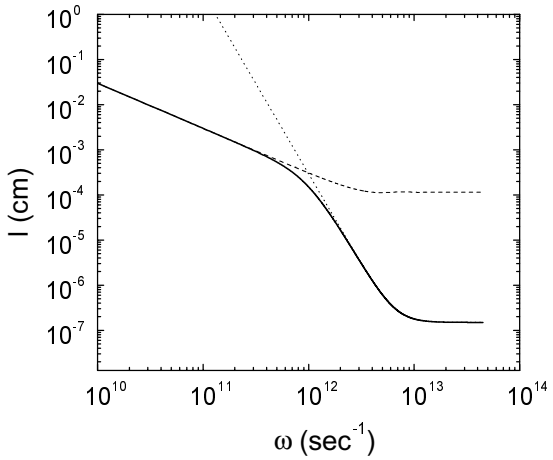

Figure 5. The phonon mean free paths l_{bi} (dashed line), l_{struc} (dotted line), and $l(\omega)$ (solid line) as functions of the frequency for a-SiO_2. The parameter set for a-SiO_2 is shown in table 1; $D = 2.6$.

It is interesting to note that equation (18) supports the empirical relation $l/\lambda \sim 150$, with λ being the wavelength of a phonon, which holds for many glasses at low temperatures (Freeman and Anderson 1986). Indeed, at low frequencies, $l \sim l_{bi}$. Expanding equation (15) at $qL \ll 1$ one gets

$$\frac{l_{bi}}{\lambda} = \frac{1}{2\pi D^2 (2\nu L)^2 n_i}. \tag{20}$$

Table 1. Parameters used for the numerical fits. The units are as follows: v_s: 10^5 cm s^{-1}; Θ_D: K; n_i: 10^{11} cm^{-2}; $2L$: 10^{-7} cm; Y: cm^{-1} K^{-4}; l_0: 10^{-7} cm.

Material	v_s	Θ_D	n_i	$2L$	ν	l_0	Y
a-SiO_2	4.1	342	2	2	0.1	1.5	1
a-GeO_2	2.6	192	2	2	0.1	0.6	2.9
a-Se	1.19	113	2	2	0.1	0.2	90
PS	1.67	123	5	2.4	0.1	0.5	80

This is a constant which depends on the model parameters which characterize the structural and elastic properties of a material. It is reasonable to assume that these parameters vary only slightly for different amorphous dielectrics (see also table 1). This can explain the observed constant-like behaviour of l/λ. In particular, for our choice of parameters for a-SiO_2, one gets $l_{bi}/\lambda \sim 135$.

To calculate κ with $l(\omega)$ from equation (18), it is convenient to use the dimensionless form of equation (14):

$$\kappa = \frac{k_B^4 T^3}{2\pi^2 \hbar^3 v_s^2} \int_0^{\Theta_D/T} x^4 e^x (e^x - 1)^{-2} l(x)\, dx \tag{21}$$

where $x = \hbar\omega/k_B T$, and the specific heat capacity is chosen in the standard Debye form. The results are shown in figure 6 and figure 7. As is seen, there is a good agreement with the experimental data over a wide temperature range. Notice that we did not use any special fitting programs to get the best fit. Instead, we have fixed the parameters related to BWDD: a dipole separation $2L = 20$ Å, the density of defects $n_i = 2 \times 10^{11}$ cm^{-2}, and the Frank index $\nu = 0.1$ (except those for PS; see table 1), and tried to bring the parameters for Rayleigh scattering close to those given by Graebner *et al* (1986). In our opinion, this provides better insight into the essence of the proposed model.

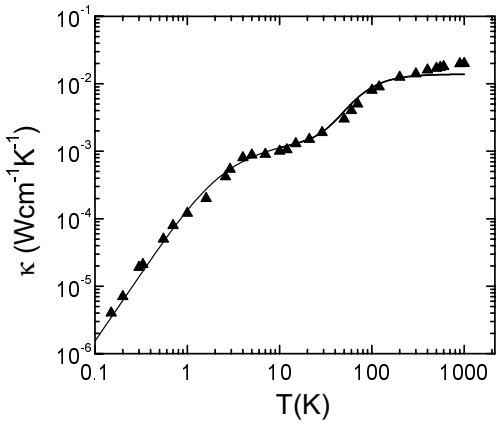

Figure 6. Thermal conductivity versus temperature for a-SiO_2 calculated according to equation (20) with $l(\omega)$ from equation (17) with a set of parameters from table 1. Experimental data from Zeller and Pohl (1971) are indicated by triangles.

4. Discussion

The results obtained in the previous section call for an additional discussion.

As is well known, a successful explanation of the thermal conductivity in amorphous dielectrics at very low temperature ($T < 1$ K) has been suggested within the phenomenological TLS model (Anderson *et al* 1972, Phillips 1972). That is, it was proposed that

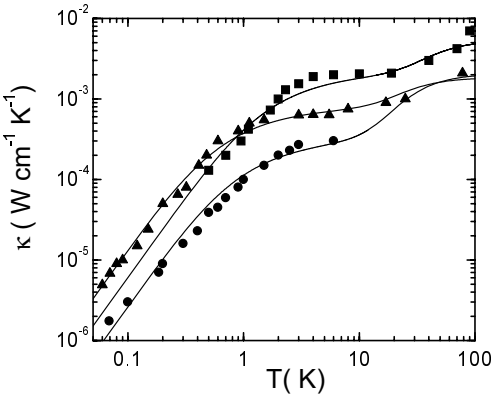

Figure 7. Thermal conductivity versus temperature for a-GeO_2 (squares), a-Se (triangles), and polystyrene (PS) (circles); the experimental data are taken from Zeller and Pohl (1971). Theoretically calculated curves are represented by solid lines. The set of model parameters is given in table 1.

at low temperatures the principal scatterers of acoustic phonons in glasses are the tunnelling states. At the same time, the universal properties of glasses in the intermediate-temperature range (the plateau region, $1 < T < 10$ K), were not understood even qualitatively within the TLS model (Freeman and Anderson 1986, Jones and Phillips 1983, Karpov and Parshin 1985). Some of these problems, however, were solved later by invoking concepts additional to that of TLS. In particular, a reasonable expression for the total phonon mean free path that allows one to describe κ over a wide temperature range reads (see for example Grannan *et al* (1988, 1990a, b), Graebner *et al* (1986))

$$l(\omega, T) = (l_t^{-1} + l_{add}^{-1} + l_R^{-1})^{-1} \tag{22}$$

where l_t and l_R are due to TLS and the Rayleigh scattering, respectively; l_{add} comes from some additional scattering mechanisms. One possible candidate considered was the phonon scattering from some kind of disorder: clusters (Graebner *et al* 1986), fractals (Alexander *et al* 1983), etc. The modern approaches involve the phonon scattering from localized low-frequency vibrations (Grannan *et al* 1988, 1990a, b, Karpov and Parshin 1985, Yu and Freeman 1987), manifesting themselves both experimentally and in computer simulations (Buchenau *et al* 1986, 1988).

Another important question is that of the low-temperature specific heat of glasses, C_v. As is known (Zeller and Pohl 1971), C_v is characterized by an anomalous linear temperature behaviour below $T < 1$ K and the excess value in the plateau region, seen as a bump in C_v/T^3 (Zeller and Pohl 1971). An explanation based on the TLS model looks quite correct at $T < 1$ K, while the extended TLS models (Grannan *et al* 1988, 1990a, b, Karpov and Parshin 1985) allow one to describe $C_v(T)$ in the plateau region.

Notice that all of these approaches are essentially based on the TLS picture. However, in spite of obvious success in interpretation of the experimental data, the original TLS model leaves some important questions unanswered. First, the microscopic basis for the TLS is unclear (Phillips 1987, Galperin *et al* 1989). Second, the quantitative universality seen in various glasses at low temperatures (for example, the above-mentioned relation $l/\lambda \sim 150$) has not been explained. Indeed, according to the TLS model

$$l/\lambda \propto (\bar{P})^{-1} \propto T_g/V_F \tag{23}$$

where $\bar{P}$ is the density of the TLS, T_g is the glass transition temperature, and V_F is the free volume frozen into the glass. However, the experimental data show that the above relation does not depend explicitly on T_g (see for example Freeman and Anderson (1986)).

In recent experiments (Xiao Liu *et al* 1997, 1998, Watson 1995), important progress has been made towards achieving an understanding of the nature of the TLS in glasses. That is, the evolution of these excitations in disordered materials has been investigated via the internal friction measurements. No difference between the low-temperature properties of amorphous and disordered solids was found. Moreover, it was shown that a *disorder* common to both disordered crystalline and amorphous phases is the primary cause of the appearance of the TLS. Thus, it has been suggested that the generation of the low-energy excitations can be understood in terms of the internal random strains which are built up with the defect density (implanted ion dose) increasing. The main conclusion of Xiao Liu *et al* (1997) is that the individual lattice defects (rather than the amorphous structure itself) play the primary role in producing the low-energy excitations.

Let us discuss these points in the context of our model. It has been demonstrated that the BWDD-induced phonon scattering combined with the Rayleigh scattering allows us to describe the thermal conductivity of various dielectric glasses over a wide temperature range. Regarding equation (23), we have shown in the previous section that the WDD-based model predicts a constant for the relation l/λ at low temperatures (see equation (20)). It is interesting that this constant depends only on the model parameters which characterize the structural properties of amorphous dielectrics.

While the question relating to the specific heat in glasses is beyond the scope of our paper, we can discuss briefly an expected contribution to the specific heat due to BWDDs. Notice that a similar problem was first considered a long time ago (Granato 1958, Couchman *et al* 1976). Granato analysed the pinned-dislocation contribution to the specific heat and found that at low temperatures (Granato 1958)

$$C_v = \frac{p\pi^2}{3}\frac{n_d a^2}{Z}\frac{Nk_BT}{\Theta_D} \tag{24}$$

where

$$p = v_s\sqrt{\rho/G}$$

(G is the shear modulus and ρ the density of a material), n_d is the dislocation density, a the lattice constant, Z the number of atoms per unit cell, and N the number of atoms per mole. This result has been discussed in connection with dielectric glasses (Couchman *et al* 1976). In particular, it was shown that there is a satisfactory agreement with the experimentally observed data for some glasses. As is known (Li 1972), with decrease of the dipole separation $2L$ the biaxial WDD becomes equivalent to an edge dislocation with the Burgers vector $b = 4L\tan(\Omega/2)$. Thus, the above result in equation (24) for dislocations should be valid also for the BWDD-based model when $2L$ is very small (which is true in our case).

As we have mentioned above, a possible explanation of the specific heat behaviour both at $T \leqslant 1$ K and $1 \leqslant T \leqslant 10$ K has been given within the extended TLS models. These approaches interpret the specific heat peculiarities in terms of the TLS states and the additional quasilocal harmonic modes. The excess harmonic modes coexisting with sound waves below 1 THz have actually been observed in glasses (Buchenau *et al* 1986, 1988). It should be recognized that the presence of localized harmonic modes is typical for elastic materials with extended defects as well. In particular, the phonon spectrum in the presence of a dislocation was shown to possess localized modes (Lifshitz and Kosevich 1966, Maradudin 1970). Also, the effect of localized vibration modes due to linear defects on the thermal properties was studied within the framework of the vibrating-string model of a dislocation (Granato 1958,

Kneezel and Granato 1982). It is clear, however, that this consideration should be accompanied by a detailed study within the BWDD model. This problem invites further investigation.

In conclusion, let us discuss a possible universality of the BWDD-based picture in glasses. Our consideration assumes the existence of new principal scatterers in disordered materials which have a clear physical origin. Indeed, as indicated above, the long-range strain fields caused by seemingly different physical objects (such as BWDDs, finite dislocation walls, and grain boundaries) are in fact identical. This allows us to include in the consideration various non-crystalline materials. In particular, the results obtained can be applied to both polycrystals and amorphous bodies. Supposedly, in disordered materials there exist randomly distributed BWDDs (small disorder corresponds to a low density of defects). This could explain the observed universal thermal properties of various materials: amorphous bodies, quasicrystals, and disordered crystals. It should be mentioned that for the amorphous dielectrics considered in our paper, the BWDD-based model supports the cluster picture proposed earlier by Phillips (1983, 1981a, b). Indeed, the best fit for the thermal conductivity gives $2L = 20$ Å as an estimate of the BWDD dipole separation, in good agreement with the predictions of the cluster model of glasses (Phillips 1983, 1981a, b). There is also some experimental evidence from neutron diffraction measurements (as well as from a study of soft breakdown in ultrathin-gate dielectrics (see for example Weir *et al* (1997)) confirming the universal character of this parameter in chalcogenide glasses (Phillips 1981a, b) and vitreous ethanol (Fayos *et al* 1996).

In metals, however, the phase with long-range orientational order and no translational symmetry has been experimentally observed by means of x-ray scattering (Shechtman *et al* 1984, Horn *et al* 1986). This finding confirms the suggestion that supercooled liquids and metallic glasses can be viewed as defected states (including disclinations) with icosahedral bond orientational order (Nelson 1983, Kléman 1989, Sadoc 1981). In particular, in two dimensions liquids are regarded as hexatic fluids interrupted by point disclinations (i.e. local points of fivefold and sevenfold symmetry) (Halperin and Nelson 1978). In accordance with this scenario (Nelson 1983, Halperin and Nelson 1978, Nelson 1982), there is a two-stage pairing process: disclinations first pair to form 5–7 dipoles regarded as dislocations, which then pair at lower temperature to form a crystalline solid. It is interesting that grain boundaries are suggested to be linear arrangements of (5–7) dipoles.

Acknowledgments

The authors wish to thank Professors J C Phillips, R O Pohl, and A C Anderson for helpful discussions and valuable comments. This work was supported by the Russian Foundation for Basic Research under grant No 97-02-16623.

Appendix A

Let us find the exact expression for the perturbation energy in equation (1). The WDD-induced strains E_{ij} can be found by using Hooke's law:

$$E_{ij} = \frac{1}{2\mu(1+\sigma)}\left[(1+\sigma)\sigma_{ij}^{d} - \sigma\sigma_{ll}^{d}\delta_{ij}\right] \tag{A.1}$$

where σ_{ij}^{d} are the stresses due to the WDD; μ and σ are the shear modulus and the Poisson constant, respectively.

For the geometry chosen in section 2 (see figure 1) the WDD-induced stresses σ_{ij}^d are (de Wit 1973)

$$\sigma_{xx}^d = \frac{\mu\Omega}{2\pi(1-\sigma)}\left[\frac{1}{2}\ln\frac{(x+L)^2+y^2}{(x-L)^2+y^2} + \frac{y^2}{(x+L)^2+y^2} - \frac{y^2}{(x-L)^2+y^2} - l_1\frac{(x+L)\big((x+L)^2-y^2\big)}{\big((x+L)^2+y^2\big)^2} + l_2\frac{(x-L)\big((x-L)^2-y^2\big)}{\big((x-L)^2+y^2\big)^2}\right] \tag{A.2}$$

$$\sigma_{yy}^d = \frac{\mu\Omega}{2\pi(1-\sigma)}\left[\frac{1}{2}\ln\frac{(x+L)^2+y^2}{(x-L)^2+y^2} + \frac{(x+L)^2}{(x+L)^2+y^2} - \frac{(x-L)^2}{(x-L)^2+y^2} - l_1\frac{(x+L)\big((x+L)^2+3y^2\big)}{\big((x+L)^2+y^2\big)^2} + l_2\frac{(x-L)\big((x-L)^2+3y^2\big)}{\big((x-L)^2+y^2\big)^2}\right] \tag{A.3}$$

$$\sigma_{zz}^d = \frac{\sigma\mu\Omega}{\pi(1-\sigma)}\left[\frac{1}{2}\ln\frac{(x+L)^2+y^2}{(x-L)^2+y^2} - l_1\frac{x+L}{(x+L)^2+y^2} + l_2\frac{x-L}{(x-L)^2+y^2}\right]. \tag{A.4}$$

Notice that equations (A.2)–(A.4) describe the stresses due to a finite wall of edge dislocations at large distances. Applying equations (A.2)–(A.4) in equation (A.1), one gets all the components of the strain tensor E_{ij} and, finally, equation (2).

Appendix B

The perturbation energy given by equation (2) takes the following form in polar coordinates:

$$U(r,\varphi) = B\left[\frac{1}{2}\ln\frac{r^2+2rL\cos\varphi+L^2}{r^2-2rL\cos\varphi+L^2} - l_1\frac{r\cos\varphi+L}{r^2+2rL\cos\varphi+L^2} + l_2\frac{r\cos\varphi-L}{r^2-2rL\cos\varphi+L^2}\right]. \tag{B.1}$$

The matrix element in equation (5) with the perturbation energy from equation (B.1) can be calculated using the following formulae:

$$\sum_{k=1}^{\infty}\frac{z^{2k-1}\cos(2k-1)\varphi}{2k-1} = \frac{1}{4}\ln\frac{1+2z\cos\varphi+z^2}{1-2z\cos\varphi+z^2} \qquad z^2 \leqslant 1 \tag{B.2}$$

$$\sum_{k=0}^{\infty} z^k\cos k\varphi = \frac{1-z\cos\varphi}{1-2z\cos\varphi+z^2} \qquad |z| < 1. \tag{B.3}$$

Substituting equations (B.2) and (B.3) into equation (B.1) and integrating in equation (5) one obtains

$$U(p,\alpha) = -\mathrm{i}\frac{4\pi BL}{pS}\left[J_0(pL)\cos\alpha + \sum_{k=1}^{\infty}(-1)^k J_{2k}(pL)\left(\frac{\cos(2k+1)\alpha}{2k+1} - \frac{\cos(2k-1)\alpha}{2k-1}\right)\right] + \mathrm{i}\frac{2\pi B}{pS}\Delta_l\left[J_0(pL)\cos\alpha + 2\cos\alpha\sum_{k=1}^{\infty}(-1)^k J_{2k}(pL)\cos 2k\alpha\right] \tag{B.4}$$

where $\Delta_l = l_1 - l_2$ and $J_m(z)$ is the Bessel function. The first term in equation (B.4) comes from the integration of the logarithmic function in equation (B.1) while the second one comes from two last terms in the r.h.s. of equation (B.1).

We have used the following standard integrals in deriving equation (B.4):

$$\int_0^{2\pi}\exp(\mathrm{i}z\cos\varphi)\cos m\varphi\,\mathrm{d}\varphi = 2\pi\mathrm{i}^m J_m(z) \tag{B.5}$$

$$\int z^k J_{k-1}(z)\,\mathrm{d}z = z^k J_k(z). \tag{B.6}$$

The first sum in equation (B.4) can be simplified by differentiation with respect to α. The second sum in equation (B.4) reads

$$\sum_{k=1}^{\infty}(-1)^k \cos(k\alpha) J_{2k}(z) = \frac{1}{2}\cos[z\cos(\alpha/2)] - \frac{1}{2}J_0(z). \tag{B.7}$$

After straightforward calculations, one obtains

$$U(p,\alpha) = \frac{B}{S}\left[-\frac{4\pi \mathrm{i}}{p^2}\sin(pL\cos\alpha) + \frac{2\pi \mathrm{i}\Delta_l}{p}\cos\alpha\cos(pL\cos\alpha)\right].$$

To find $\mathcal{R}(\theta)$ in equation (4) one has to average $|U(p,\alpha)|^2$ over α:

$$\begin{aligned}|U(p)|^2 = \overline{|\langle \boldsymbol{q}|U(\boldsymbol{r})|\boldsymbol{q}'\rangle|^2} &= \frac{1}{2\pi}\int_0^{2\pi}|U(p,\alpha)|^2\,\mathrm{d}\alpha \\ &= \frac{2\pi B^2}{S^2}\int_0^{2\pi}\left(\frac{4}{p^4}\sin^2(pL\cos\alpha) - \frac{2\Delta_l}{p^3}\cos\alpha\sin(2pL\cos\alpha)\right. \\ &\quad \left. + \frac{\Delta_l^2}{p^2}\cos^2\alpha\cos^2(pL\cos\alpha)\right)\mathrm{d}\alpha.\end{aligned} \tag{B.8}$$

Using

$$\int_0^{2\pi}\begin{pmatrix}\cos(z\cos\alpha)\\ \sin(z\cos\alpha)\end{pmatrix}\cos(n\alpha)\,\mathrm{d}\alpha = 2\pi\begin{pmatrix}\cos(n\pi/2)\\ \sin(n\pi/2)\end{pmatrix}J_n(z) \tag{B.9}$$

one finally gets

$$\begin{aligned}|U(p)|^2 = \frac{4\pi^2 B^2}{S^2}\left\{\frac{2}{p^4}\big(1 - J_0(2pL)\big) - \frac{2\Delta_l}{p^3}J_1(2pL)\right. \\ \left. + \frac{\Delta_l^2}{2p^2}\left(\frac{1}{2} + J_0(2pL) - \frac{J_1(2pL)}{2pL}\right)\right\}.\end{aligned} \tag{B.10}$$

Substituting equation (B.10) into equation (4) one obtains the effective differential scattering radius in equation (6).

The exact expression for the mean free path in equation (3) takes the form

$$\Lambda^{-1} = \frac{n_i B^2 \pi}{\hbar^2 v^2}\left\{\frac{1}{2q^3}I_1(qL) + \frac{\Delta_l^2}{2q}I_2(qL) - \frac{\Delta_l}{q^2}I_3(qL)\right\} \tag{B.11}$$

where

$$\begin{aligned}I_1(qL) &= \int_0^{2\pi}\frac{\mathrm{d}\theta}{\sin^2(\theta/2)}\,(1 - J_0(4qL\sin(\theta/2)) \\ &= 16q^2L^2\pi\big(J_0^2(2qL) + J_1^2(2qL)\big) - 8qL\pi J_0(2qL)J_1(2qL)\end{aligned} \tag{B.12}$$

$$\begin{aligned}I_2(qL) &= \int_0^{2\pi}\left(\frac{1}{2} + J_0(4qL\sin(\theta/2)) - \frac{J_1(4qL\sin(\theta/2))}{4qL\sin(\theta/2)}\right)\mathrm{d}\theta \\ &= 2\pi\left(\frac{1}{2} + J_0^2(2qL)\right) - \pi\big(J_0^2(2qL) + J_1^2(2qL)\big)\end{aligned} \tag{B.13}$$

$$I_3(qL) = \int_0^{2\pi}\frac{\mathrm{d}\theta}{\sin(\theta/2)}\,J_1(4qL\sin(\theta/2)) = 4qL\pi\big(J_0^2(2qL) + J_1^2(2qL)\big). \tag{B.14}$$

The final result for the mean free path is given by equation (7).

References

Alexander S, Laermans C, Orbach R and Rothenberg H M 1983 *Phys. Rev.* B **28** 4615
Amelinckx S 1959 *Phil. Mag.* **1** 269
Anderson A C and Malinowski M E 1972 *Phys. Rev.* B **17** 3199
Anderson P W, Halperin B I and Varma C M 1972 *Phil. Mag.* **25** 1
Berman R 1952 *Proc. Phys. Soc.* **65** 1029
Blewitt T H, Colman R R and Redman J K 1954 *Phys. Rev.* **93** 891
Buchenau U, Prager M, Nücker N, Dianoux A J, Ahmad N and Phillips W A 1986 *Phys. Rev.* B **34** 5665
Buchenau U, Zhou H M, Nücker N, Gilroy K S and Phillips W A 1988 *Phys. Rev. Lett.* **60** 1318
Couchman P R, Reynolds C L and Cotterill R M J 1976 *Nature* **259** 108
de Wit R 1973 *J. Res. NBS* A **77** 607
Fayos R, Bermejo F J, Dawidowski J, Fischer H E and González M A 1996 *Phys. Rev. Lett.* **77** 3823
Freeman J J and Anderson A C 1986 *Phys. Rev.* B **34** 5684
Galperin Y M, Karpov V G and Kozub V I 1989 *Adv. Phys.* **38** 669
Gantmakher V F and Levinson Y B 1987 *Carrier Scattering in Metals and Semiconductors* (Amsterdam: North-Holland)
Graebner J E, Golding B and Allen L C 1986 *Phys. Rev.* B **34** 5696
Granato A 1958 *Phys. Rev.* **111** 740
Grannan E R, Randeria M and Sethna J P 1988 *Phys. Rev. Lett.* **60** 1402
Grannan E R, Randeria M and Sethna J P 1990a *Phys. Rev.* B **41** 7784
Grannan E R, Randeria M and Sethna J P 1990b *Phys. Rev.* **41** 7799
Gusev A I 1998 *Usp. Fiz. Nauk* **168** 55
Halperin B I and Nelson D R 1978 *Phys. Rev. Lett.* **41** 121
Horn P M, Malzfeldt W, DiVincenzo D P, Toner J and Gambino R 1986 *Phys. Rev. Lett.* **57** 1444
Jones D P and Phillips W A 1983 *Phys. Rev.* B **27** 3891
Jones D P, Thomas N and Phillips W A 1978 *Phil. Mag.* B **38** 271
Karpov V G and Parshin D A 1985 *Zh. Eksp. Teor. Fiz.* **88** 2212
Kauzmann W 1948 *Chem. Rev.* **43** 219
Kléman M 1983 *Points, Lines and Walls in Liquid Crystals, Magnetic Systems and Various Ordered Media* (New York: Wiley)
Kléman M 1989 *Adv. Phys.* **38** 605
Klemens P G 1955 *Proc. Phys. Soc.* **68** 1113
Kneezel G A and Granato A V 1982 *Phys. Rev.* B **25** 2851
Krasavin S E and Osipov V A 1997 *Phys. Lett.* A **236** 245
Li J C M 1960 *Acta Metall.* **8** 563
Li J C M 1972 *Surf. Sci.* **31** 12
Li J C M and Gilman J J 1970 *J. Appl. Phys.* **41** 4248
Lifshitz I M and Kosevich A M 1966 *Rep. Prog. Phys.* **29** 217
Liu Xiao, Vu P D, Pohl R O, Schiettekatte F and Roorda S 1998 *Phys. Rev. Lett.* **81** 3171
Liu Xiao, White B E Jr, Pohl R O, Iwanizcko E, Jones K M, Mahan A H, Nelson B N, Crandall R S and Veprek S 1997 *Phys. Rev. Lett.* **78** 4418
Maradudin A A 1970 Localized vibration modes associated with screw dislocations *Fundamental Aspects of Dislocation Theory (NBS Special Publication 317)* Part I (Washington, DC: US Government Printing Office) pp 205–17
Nelson D R 1982 *Phys. Rev.* B **26** 269
Nelson D R 1983 *Phys. Rev.* B **28** 5515
Osipov V A and Krasavin S E 1998a *J. Phys. C: Solid State Phys.* **10** L639
Osipov V A and Krasavin S E 1998b *Phys. Lett.* A **250** 369
Phillips J C 1981a *Phys. Rev.* B **24** 1744
Phillips J C 1981b *J. Non-Cryst. Solids* **43** 37
Phillips J C 1983 *Solid State Physics* vol 37, ed H Ehrenreich and D Turnbull (New York: Academic) p 93
Phillips W A 1972 *J. Low Temp. Phys.* **7** 351
Phillips W A 1987 *Rep. Prog. Phys.* **50** 1657
Randeria M and Sethna J P 1988 *Phys. Rev.* B **38** 12 607
Read W T and Shockley W 1950 *Phys. Rev.* **78** 275
Rider J G and Foxon C T B 1967 *Phil. Mag.* **16** 1133
Rivier N 1979 *Phil. Mag.* A **40** 859

Roth E P and Anderson A C 1978 *Phys. Rev.* B **17** 3356
Sadoc J F 1981 *J. Non-Cryst. Solids* **44** 1
Shechtman D, Blech I, Gratias D and Cahn J W 1984 *Phys. Rev. Lett.* **53** 1951
Watson S K 1995 *Phys. Rev. Lett.* **75** 1965
Weilert M A, Msall M E, Wolfe J P and Anderson A C 1993 *Z. Phys.* B **91** 179
Weir B E, Silverman P J, Monroe D, Kirsch K S, Alam M A, Alers G B, Sorsch T W, Timp G L, Baumann F, Liu C T, Ma Y and Hwang D 1997 Ultra-thin gate dielectrics: they break down, but do they fail? *IEDM Technical Digest* (:) p 73
Yu C C and Freeman J J 1987 *Phys. Rev.* B **36** 7620
Zeller R C and Pohl R O 1971 *Phys. Rev.* B **4** 2029
Ziman J M 1960 *Electrons and Phonons: the Theory of Transport Phenomena in Solids* (Oxford: Clarendon)